Performance analysis of a high-efficiency multi-bed active magnetic regenerator device

Masche, M.; Liang, J.; Dall'Olio, S.; Engelbrecht, K.; Bahl, C.R.H.

Published in:
Applied Thermal Engineering

Link to article, DOI:
10.1016/j.applthermaleng.2021.117569

Publication date:
2021

Document Version
Peer reviewed version

Journal Pre-proofs

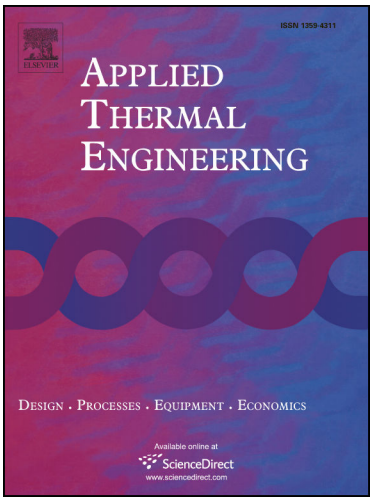

Performance analysis of a high-efficiency multi-bed active magnetic regenerator device

M. Masche, J. Liang, S. Dall'Olio, K. Engelbrecht, C.R.H. Bahl

PII: S1359-4311(21)00998-4
DOI: https://doi.org/10.1016/j.applthermaleng.2021.117569
Reference: ATE 117569

To appear in: *Applied Thermal Engineering*

Received Date: 21 May 2021
Revised Date: 9 August 2021
Accepted Date: 11 September 2021

Please cite this article as: M. Masche, J. Liang, S. Dall'Olio, K. Engelbrecht, C.R.H. Bahl, Performance analysis of a high-efficiency multi-bed active magnetic regenerator device, *Applied Thermal Engineering* (2021), doi: https://doi.org/10.1016/j.applthermaleng.2021.117569

Performance analysis of a high-efficiency multi-bed active magnetic regenerator device

M. Masche[1,*], J. Liang[1], S. Dall'Olio[2], K. Engelbrecht[1], C.R.H. Bahl[1]

[1]Department of Energy Conversion and Storage, Technical University of Denmark (DTU), Anker Engelunds Vej B301, 2800 Kgs. Lyngby, Denmark

[2] Faculty of Mechanical Engineering, University of Ljubljana, Aškerčeva 6, SI-1000 Ljubljana, Slovenia

*Corresponding author. E-mail: marv@dtu.dk

Abstract

We present the performance of an active magnetic regenerator prototype with a multi-bed concept and parallel flow circuit. The prototype applies a two-pole permanent magnet (maximum magnetic flux density of 1.44 T) that rotates over 13 tapered regenerator beds mounted on a laminated iron yoke ring. Each bed is filled with about 260 g of spherical particles, distributed in layers of ten alloys of $La(Fe,Mn,Si)_{13}H_y$ (CALORIVAC HS) with different Curie temperatures. Other important features are the solenoid valves, the monitoring of the temperatures exiting each bed at the cold side, and a torque meter used to measure the magnetic power required to drive the cycle. The opening behavior of the solenoid valves (i.e., the blow fraction) could be adjusted to correct flow imbalances in each bed. The device provided a maximum cooling power of about 815 W at a cycle frequency of 1.2 Hz, a utilization of 0.36, and a hot reservoir temperature of 295 K while maintaining a 5.6 K-temperature span with a coefficient of performance of 6.0. In this case, the second-law efficiency was 11.6 %. The maximum second-law efficiency of 20.5 %, which represents one of the largest for a magnetocaloric device, was obtained at a cycle frequency of 0.5 Hz, a utilization of 0.34, and a hot reservoir temperature of 295 K at a temperature span of 10.3 K. Under these conditions, the device absorbed a cooling load of 288 W with a coefficient of performance of 5.7. It was also shown that an unbalanced flow due to different hydraulic resistance through the beds can cause cold side outlet temperature variations, which reduce the system performance, demonstrating the importance of a well-functioning, balanced flow system.

Keywords: magnetocaloric effect; cooling performance; active magnetic regenerator; first-order phase transition

Nomenclature

Acronyms

AMR	Active Magnetic Regenerator	MCE	Magnetocaloric Effect
COP	Coefficient of Performance	MCM	Magnetocaloric Material
DTU	Technical University of Denmark	RTD	Resistance Temperature Detector
FOPT	First-Order Phase Transition	TC	Thermocouple
GWP	Global Warming Potential	TSM	Taylor Series Method

Symbols

$\dot{Q}_h$	Heating power - supplied heat [W]	Gd	Gadolinium
$\dot{Q}_c$	Cooling power [W]	m	Mass [kg]
$\dot{W}_{losses}$	Iron losses [W]	p	Pressure [bar]
$\dot{W}_{mag}$	Magnetic power into regenerator [W]	T	Temperature [K]
$\dot{W}_{pump}$	Pumping power [W]	T_{cold}	Cold reservoir temperature [K]
$\dot{W}_{shaft}$	Shaft power [W]	T_{Curie}	Curie temperature [K]
$\dot{V}$	Volumetric flow rate [L h^{-1}]	T_{hot}	Hot reservoir temperature [K]
Δp	Pressure drop [bar]	U	Utilization factor [-]
ΔT	Temperature span, T_{hot}-T_{cold} [K]	η_{II}	Second-law efficiency [%]
c_p	Specific heat capacity [J·kg^{-1}·K^{-1}]	ρ	Density [kg m^{-3}]
d	Diameter [μm]	Γ	Shaft torque [N m]
f	Operating (motor) frequency [Hz]	τ	AMR cycle period [s]
F_b	Blow fraction [%]	τ_b	Single blow period [s]

Subscripts

ad	Adiabatic	max	Maximum
c	Cooling	p	Particle
f	Fluid	Reg	Regenerator
h	Heating	s	Solid refrigerant

1. Introduction

Currently, all our heating and cooling needs are almost exclusively met by conventional vapor compression cooling/heating systems, which use gaseous refrigerants with ozone depletion and global warming potential (GWP) [1,2]. At the same time, global energy demand has been increasing rapidly due to intensive urbanization, population growth, and improved living standards across the globe. A considerable amount of energy is consumed for space heating and cooling, resulting in significant greenhouse gas emissions [3]. Therefore, there is great interest in employing energy-saving systems that reduce emissions from this sector while also providing safe and robust operation and environmentally benign refrigerants. One of the most promising technologies that fit these requirements are solid-state caloric heat pumps [4,5], in particular, heat pumps utilizing the active magnetic regenerator (AMR) concept [6,7], a concept first introduced by Barclay [8].

Heat pumps based on the AMR concept use the reversible magnetocaloric effect (MCE) of solid-state refrigerants, the so-called magnetocaloric material (MCM) that have no direct GWP [2], in order to build a cooling/heating cycle. The AMR cycle comprises four operational steps: 1) magnetization, which causes the MCM to heat up, 2) the cold-to-hot-blow (or cold blow), where the heat transfer fluid is pumped from the cold side to the hot side in order to reject the magnetic work to the surroundings, 3) demagnetization, which causes the MCM to cool down and 4) the hot-to-cold blow (or hot blow), where the fluid is pumped from the hot side to the cold side to absorb a cooling load. The timing of each of these four steps is important for the performance of the system. Varying the synchronization between the magnetic and fluid flow profile can be performance-enhancing [9,10]. The possibility to synchronize the fluid blow with the magnetization/demagnetization leads to the important definition of the blow fraction (F_B), which is the time fraction of the AMR cycle when fluid is blown through the regenerator [11,12].

The performance of the AMR cycle is highly influenced by the coupling between the magnetic circuit, flow system, and regenerator. Hence, parameters related to the magnetic circuit (e.g., magnet mass, flux density, number of poles, cycle frequency), the flow system (e.g., heat transfer fluid, flow rate, valve friction), and the regenerator (e.g., mass and type of MCM, porosity, shape, effectiveness) must be considered for evaluating the AMR performance. A number of devices with a wide range of design concepts based on the AMR cycle have been built and tested, see, for example [13,14,23,15–22]. Most devices use pure gadolinium (Gd) as a working material. Gd has a second-order phase transition and exhibits the MCE near room temperature [24,25]. In comparison, first-order phase transition (FOPT) refrigerants have the advantage of exhibiting a large isothermal entropy change and hence a large MCE, which is needed to achieve higher cooling capacities than Gd [26], especially when the temperature span is below 30 K [27].

Lanthanum-based materials with a FOPT have attracted great interest as refrigerant candidates in magnetocaloric cooling applications owing to their large MCE, low cost, and continuously adjustable Curie temperature (T_{Curie}) [25]. The potential of FOPT-based AMRs was demonstrated by Jacobs et al. [28], who built a 1.44-T cooling unit featuring twelve multi-layered regenerators filled with a total of 1.52 kg of LaFeSiH. At 4 Hz, the unit produced a promising zero-span cooling power of 3042 W and a peak cooling power of 2502 W over an 11.0 K span with an electrical coefficient of performance (*COP*) of 1.9. Later, rotary AMR devices have been reported that also use multi-bed regenerators filled with FOPT alloys, such as LaFeSi [29], LaFeMnSiH [30,31], or manganese-based alloys [32]. Recently, Maier et al. [33] demonstrated a zero-span specific cooling power of 12.5 W g^{-1} at 20 Hz for a 1.2-T magnetic refrigerator, employing a $La(FeMnSi)_{13}$-based MCM in a single regenerator, albeit using a different conceptual setup

than conventional AMR devices. A comprehensive list of rotary AMR devices presented before 2019 is described in review articles [34–36], reporting around 80 AMR prototypes.

The control and operation of the hydraulic system are important aspects in achieving optimum AMR performance. Recent studies [37–42] suggest that imbalances in the heat transfer fluid flow significantly affect the AMR performance, and optimal blow fractions are beneficial in terms of the cooling capacity. For example, Holladay et al. [42] encountered flow imbalances as a result of different fluid masses being displaced during the cold (low-field) blow and hot (high-field) blow, resulting in several percent of the cold fluid being bypass around the magnetized regenerator. Furthermore, Eriksen et al. [38] could balance flow imbalances by adjusting the valves controlling the flow entering and leaving the hot side, resulting in a significant increase in the temperature span.

This study aims to demonstrate an efficient operation of a rotary AMR system using ten alloys of a commercial $La(Fe,Mn,Si)_{13}H_y$ refrigerant. This paper presents the cooling performance of a multi-bed AMR prototype for different operating frequencies (ranging from 0.5 to 1.2 Hz) and utilization factors (ranging from 0.27 to 0.40). In this work, we present the magnetic properties of the MCM in detail. Special attention has also been given to analyze the influence of the opening behavior of the solenoid valves (i.e., the blow fraction) on the system performance.

2. Experimental work

2.1. AMR apparatus

The AMR prototype was developed at DTU and is called MagQueen. Initially, it was developed during the ENOVHEAT project (Innovation Fund Denmark 2013-2018) for heat pump applications to provide, for example, the heating needs of a low-energy single-family house in Denmark with a higher *COP* than traditional systems [31,43,44]. In the RES4BUILD project, which brings together 15 partners across research institutes and industry, MagQueen is part of an integrated renewable energy-based system that aims to decarbonize the energy consumption in buildings. Table 1 lists the technical specifications of the AMR prototype.

Table 1: Specifications of the AMR prototype.

Property	Value
AMR type	Rotary
Magnet system	Two-pole permanent magnet
Average high field flux density	1.44 T
Air gap	23 mm
Flow system	Parallel flow
Heat transfer fluid	Water mixed with 2 vol.% ENTEK FNE
Flow control	Solenoid valves based on magnet shaft encoder position
Regenerator characteristics	
Number of beds	13
Bed volume	60.3 cm^3, 0.059 m long, 0.017 m height
Bed tapering angle	-10°
Number of layers	10

Refrigerant material	$La(Fe,Mn,Si)_{13}H_y$
Bed porosity	0.38
Refrigerant mass	262 g (3.41 kg in total)
Bed type	Packed spheres
Particle diameters	0.4-0.63 mm

The MagQueen is shown in Figure 1. It is a 13 bed AMR with a rotating two-pole permanent magnet. The regenerator beds are trapezoid-shaped, and the negative tapering angle indicates that the cross-section of the regenerator at the cold side is larger than the one at the hot side. Each bed is mounted on top of an iron tooth. The entire permanent magnet assembly is mounted on a rotor above the bed, and the magnetic flux is guided through a laminated iron ring mounted below the regenerator beds. An absolute rotary encoder attached to the motor shaft monitors the angular position of the spinning magnet. A torque meter measures the shaft work from the electric motor. The fluid flow is controlled by 26 solenoid valves mounted on the hot side of the regenerator bed and 26 check valves on the cold side. More details of the AMR design are given in [31,45].

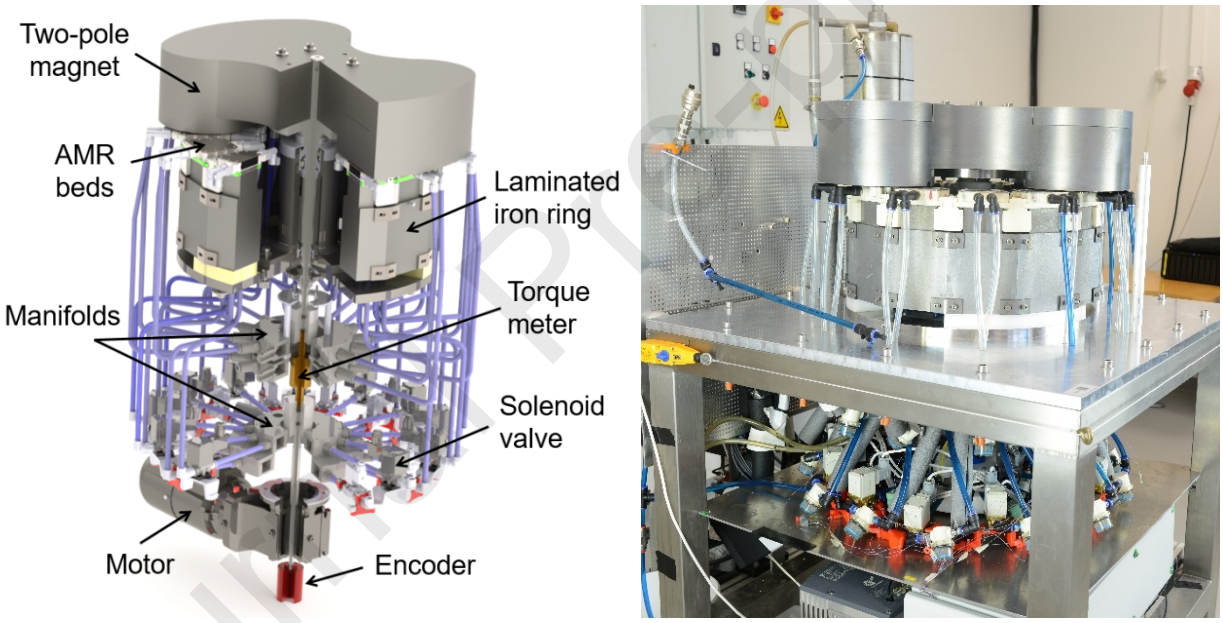

Figure 1: (a) Schematic section view and (b) photograph of MagQueen fully assembled.

A simplified schematic of the flow system is shown in Figure 2. The parallel fluid flow circuit in MagQueen consists of solenoid valves, flow strainers with filters, a pump, check valves, and manifolds, allowing for continuous flow of the heat transfer fluid through the system while ensuring a reciprocating flow in each regenerator bed. The heat transfer fluid is water mixed with 2 vol.-% ENTEK FNE, a corrosion inhibitor, to avoid oxidation of the iron-based MCM. The flow in each bed is controlled using two solenoid valves and two check valves, with the solenoid valves mounted on the hot side of the regenerators. The working fluid is circulated by a centrifugal pump, which connects the AMRs with the external (heat sink and heat source) heat exchangers. On the cold reservoir (connected to the heat source) of MagQueen, the cold outlet fluid

flows through a circulation heater, which simulates the cooling load. After the fluid has warmed up by passing through the magnetized AMRs (i.e., the cold blow), the fluid is cooled down to its initial temperature to simulate a steady-state magnetocaloric cooling cycle. Hence, the hot outlet fluid flows through a chiller, which controls the hot reservoir temperature via a counter-flow plate heat exchanger at the hot reservoir (connected to the heat sink) before returning to the regenerator hot inlet.

There are four manifolds (i.e., two hot side and two cold side manifolds) with pressure meters installed, where the working fluid is collected after exiting the regenerators or distributed into the regenerators. The encoder continuously measures the magnet position, which controls the opening of the solenoid valves, and hence the blow fraction (i.e., the flow waveform) (Figure 3). Hence, the solenoid valves can control the reciprocating fluid flow through each regenerator synchronized with the periodically changing external magnetic field. The valve-opening angle can be modified while the system is in operation to regulate the internal flow profile through each regenerator bed. The way the fluid blows through the AMR, the flow profile, and its coupling with the magnetic field largely affect the AMR performance. Based on the results from [11,40,41,46,47], the timing and duration of the blow period significantly affect the AMR performance. Hence, the blow fraction (F_b) can be defined as follows:

$$F_b = \frac{2\tau_b}{\tau}, \qquad \textit{Eq. 1}$$

Where τ_b and τ denote the duration of a single period of one fluid blow and the whole AMR cycle, respectively, see Figure 3, which shows the profiles of the generic magnetic flux density and the fluid flow profile. Only the variation of the cold-to-hot blow fraction is shown, which can be adjusted by varying the opening of the solenoid valves connected to the hot outlet of the AMR bed. The higher blow fraction stands for a longer opening of the solenoid valves and hence leads to a reduction of the system pressure.

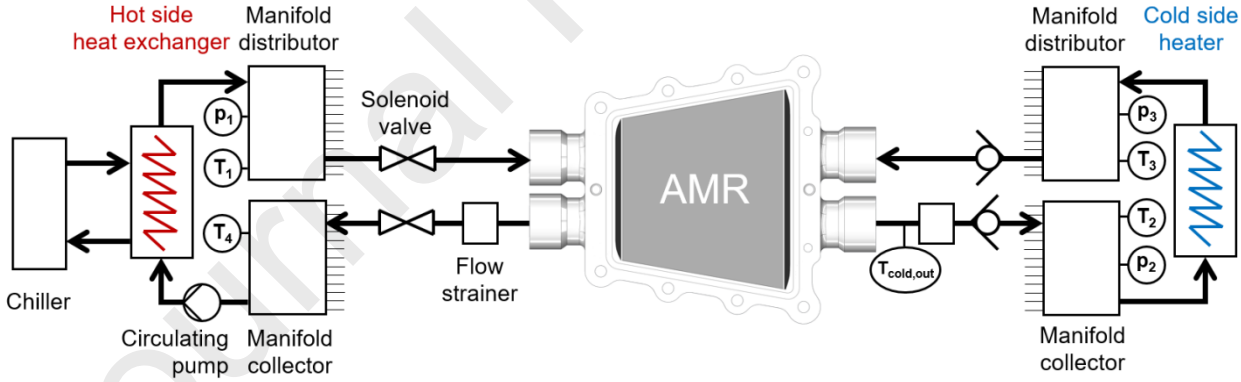

Figure 2: Schematic view of the heat transfer fluid flowing through one AMR bed.

The circulation heater and tubing carrying the cold working fluid were insulated to prevent heat leaks to the ambient. Fluid temperatures were measured on the cold side exiting the AMR ($T_{cold,out}$) using thermocouples (TCs), and temperatures inside the four manifolds were obtained from resistance temperature detectors (RTDs). The temperature sensors (TCs and RTDs) were calibrated in an isothermal bath close to a precision thermometer, and sensors of the same type (TC or RTD) were calibrated simultaneously. The accuracy of the E-type TCs and RTDs after calibration was less than ± 0.3 °C and ± 0.08 °C, respectively. As shown in Figure 2, T_1 refers to the temperature of the fluid entering the regenerator from the hot side during the hot blow, and it is assumed equal to the hot reservoir

temperature (T_{hot}). T_2 is the temperature of the fluid exiting the regenerator at the cold end during the hot blow. It is the lowest fluid temperature in the AMR cycle. T_3 is the temperature entering the regenerator from the cold side during the cold blow and is assumed equal to the cold reservoir temperature (T_{cold}). T_4 is the temperature exiting the regenerator at the hot side during the cold blow. It represents the highest fluid temperature in the AMR cycle. The difference between the T_{hot} and T_{cold} is referred to as the reservoir temperature span (ΔT) of the system. Table 2 lists the characteristics of the quantities measured in the AMR setup and their accuracies.

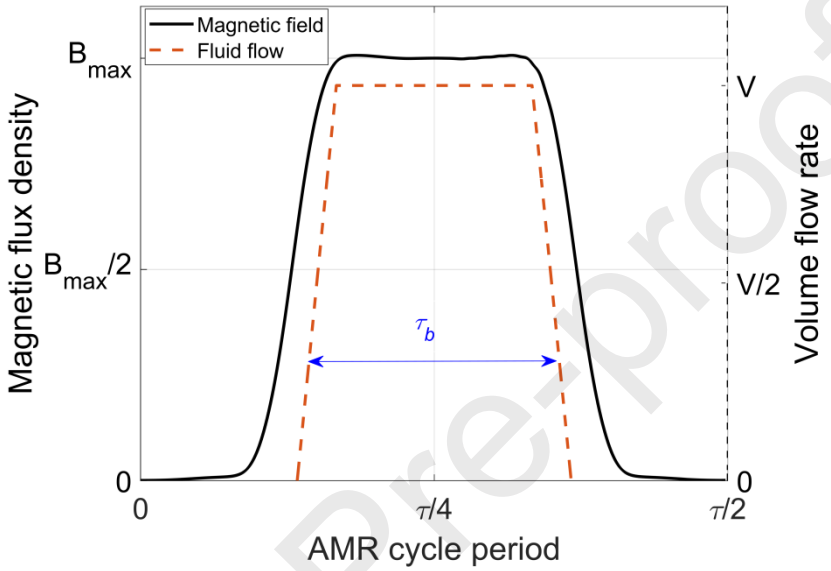

Figure 3: Generic magnetic flux density profile (solid line) and fluid flow profile (dashed line) of the AMR cycle. For simplicity, only the cold-to-hot blow fraction at one high field is shown.

Table 2: Sensors in the AMR apparatus and their accuracy provided by the manufacturer.

Measurement	Characteristics (type)	Accuracy[1]
Temperature	RTD (Pt100)	± (0.15 + 0.002 T) °C
	Thermocouple (E)	± 0.5 K
Torque	Rotary torque sensor	± 1 % of torque
Pressure	Pressure transmitter	± 0.3 % of pressure
Fluid flow rate	High range (5.7-56.8 L/min) flow meter (liquid flow transmitter)	± 2 % of flow
	Low range (0.5-10 L/min) flow meter (vortex)	± 1 % of flow
Cycle frequency	Frequency inverter	± 0.5 % of frequency
Magnet position	Absolut analog encoder	± 0.07 % of angle

[1]Rectangular (uniform) probability distributions are assumed in the accuracy component.

The chiller and heater could be adjusted to simulate various heat load conditions. The entire prototype was controlled via LabVIEW software, which was also responsible for data acquisition and storage. The errors introduced from the data acquisition were considered to be relatively small. By setting the AMR

frequency, the magnet started rotating. The flow rate, encoder angle, torque, pressure, and temperatures were monitored continuously. Several outputs were recorded by the software, such as temperatures, shaft power, pumping power, temperature span, and cooling power. The sampling frequency of the measured parameters was about 6 Hz. For each set of experiments, the presented data were averaged over a period of 10 min after reaching steady-state operating conditions, leading to 3,600 measurements. The steady-state operation was obtained when the standard deviation of the measured reservoir temperature span was below 0.05 K for more than 2 min.

2.2. Regenerator characteristics

Each AMR bed was filled with spherical particles of ten alloys of the FOPT material $La(Fe,Mn,Si)_{13}H_y$ (CALORIVAC-HS, CV-HS) provided by Vacuumschmelze GmbH & Co. KG (Germany). The CV-HS material had an increased α-Fe content compared to CV-H, which enhances stability and integrity, as described in detail in [48]. Liang et al. [48] showed that AMRs with loose particles of $La(Fe,Mn,Si)_{13}H_y$ could outperform AMRs with epoxy-bonded particles of $La(Fe,Mn,Si)_{13}H_y$ in terms of higher heat transfer and reduced internal dead volume, thus leading to higher cooling performance. Thus, the beds were filled without epoxy bonding of the particles. The mass and T_{Curie} distribution of the ten alloys is listed in Table 3. This distribution of T_{Curie} was chosen according to the temperature requirements within the RES4BUILD project, although there was some variation between the design T_{Curie} and the manufactured materials.

Table 3: Distribution of Curie temperatures, peak temperature (T_{peak}) at the maximum adiabatic temperature change ($\Delta T_{ad,max}$) for a magnetic field change of 1.5 T, and refrigerant mass across the regenerator bed.

Layer	1 (hot)	2	3	4	5	6	7	8	9	10 (cold)
T_{Curie} (K)	292.1	290.1	288.7	287.0	283.8	282.6	280.6	278.4	275.8	273.1
T_{peak} *at* $\Delta T_{ad,max}$ (K)	293.9	291.9	290.2	289.2	285.6	284.4	282.4	280.2	277.6	274.9
Mass (g)	40.5	29.0	25.5	28.0	23.0	22.5	19.0	21.0	25.0	30.5

Before the materials were installed in the system, their magnetocaloric properties were measured. The specific heat capacity was measured using a custom-built differential scanning calorimeter with an applied magnetic field [49]. Figure 4a shows the average specific heat capacity curves obtained under cooling and heating of two specific MCMs. The curves show a clear field dependence, which is characteristic of a FOPT material [50]. The T_{Curie} was defined as the temperature of the narrow peak in the specific heat capacity at zero magnetic field. The difference between the specific heat capacity peak under cooling and heating was around 1 K, indicating a small thermal hysteresis of the MCMs.

Figure 4b presents the MCE of each layer characterized by the adiabatic temperature change (ΔT_{ad}) when magnetized from 0 to 1.5 T. The measurement technique for the determination of the ΔT_{ad} is described in detail in [51]. The curves for the ΔT_{ad} are caret shaped, and the measured peak (T_{peak}) of the ΔT_{ad} changes systematically between the ten different alloys, indicating that it is tunable. In general, accurate tailoring

of the structural transition temperature of the $La(Fe,Mn,Si)_{13}H_y$ material can be realized by varying the composition, e.g., the ratio of Mn to Si. However, it is also shown that the spacing between the values of T_{peak} for the different layers is not even, due to manufacturing tolerances in the precise tailoring. It is noted that the maximum of the ΔT_{ad} is not at T_{Curie}. This is because of the magnetic field dependence of the structural transition of the FOPT material, which means that T_{peak} increases with the applied magnetic field.

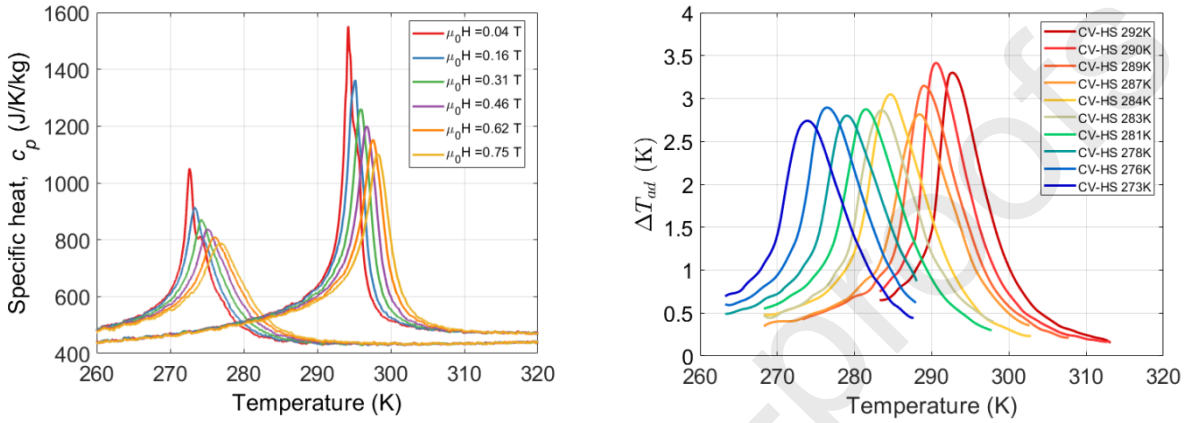

(a) (b)

Figure 4: (a) The specific heat capacity curves for the MCM layers with the coldest and hottest T_{Curie}. (b) The adiabatic temperature change of each of the ten layers as a function of temperature when magnetized from 0 to 1.5 T. Data provided by Vacuumschmelze GmbH & Co. KG.

The pressure drop through each of the 13 AMRs was measured as a function of the fluid flow rate to assess the uniformity of the flow resistance in each regenerator and evaluate the packing quality. The difference between the pressure at the inlet (cold side) and outlet (hot side) of the regenerator housing are shown in Figure 5. Preliminary tests performed on a single regenerator showed no difference in the pressure drop between pumping the fluid in the converging (cold blow) or diverging (hot blow) housing direction. Hence, the data presented in Figure 5 only shows the data for the converging flow process. The fluid flow rate was controlled using a needle valve, and the pressure response was monitored using a pressure gauge. Therefore, only horizontal box plots were shown. It can be seen that the flow rate needed to obtain a specific pressure drop through each bed varied, indicating different flow path resistances of the beds. The manual filling of the layered MCM and differences in fittings, tubing, and housing may explain the flow variations between the AMR beds. Overall, the 13 beds had an average porosity of 38 (±0.6) %, indicating a similar packing structure among the beds. The porosity was measured as the ratio of pore volume to regenerator (bulk) volume.

The predicted pressure drop across a packed bed was also evaluated by means of an empirical Ergun equation [52] assuming a bed with smooth particles [53]. Figure 5 also shows the averaged curve from all 13 beds compared to the pressure drop across the AMR bed containing particles having the smallest diameter (d_p = 400 µm) and largest diameter (d_p = 630 µm). It is shown that the experimental data are closer to the pressure drop predicted by the Ergun equation for d_p = 630 µm, which is at the upper end of the particle size range. The better fit of the experimental data with the Ergun plot for larger particles is

possibly due to particles not being perfectly spherical, as shown in Dall'Olio et al. [45]. It was shown that the Ergun equation predicts satisfactorily the pressure drop in packed beds for spherical particles over a wide range of flow rates. At the same time, it systematically under-predicts the pressure drop over non-spherical (cylinder-like) particles [54].

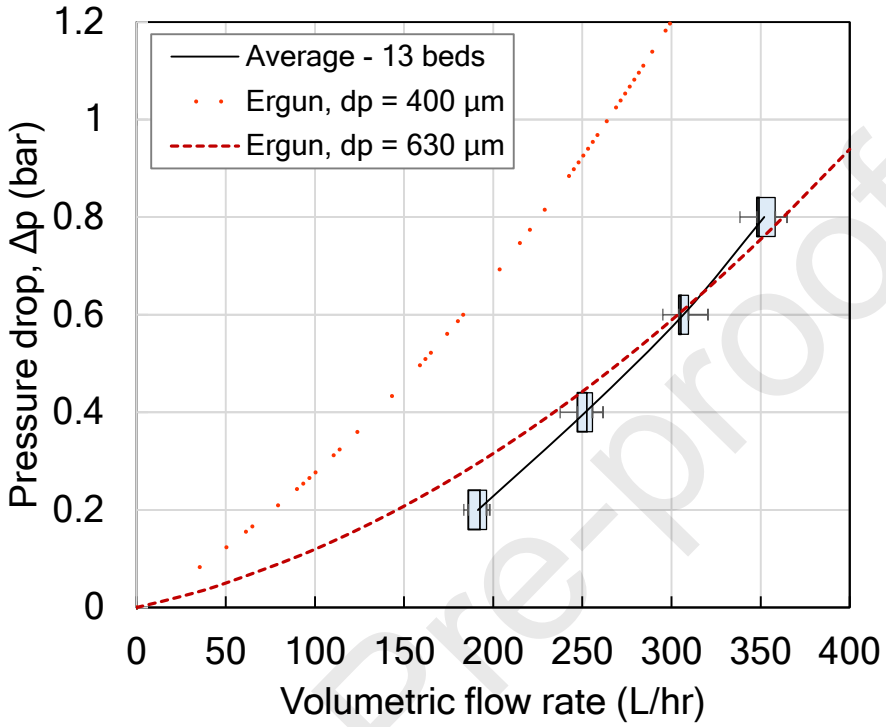

Figure 5: Pressure drop vs. fluid volumetric flow rate for the 13 AMR beds in comparison to the predicted pressure drop by Ergun's equation. Boxplots indicate the median of the measured data between the first and third quartiles, and whiskers show the lowest and highest value.

3. Performance measure definitions

The thermodynamic efficiency of the AMR device was evaluated by the cooling power, the cooling *COP*, and the second-law efficiency. The cooling *COP* of the actual AMR that only takes into account the net input power was defined as follows:

$$COP = \frac{\dot{Q}_c}{\dot{W}_{mag} + \dot{W}_{pump}} \qquad \textit{Eq. 2}$$

The cooling power ($\dot{Q}_c$) was calculated based on the temperature change of the fluid across the heater on the cold side:

$$\dot{Q}_c = \dot{V}\, \rho_f\, c_f\, \Delta T_{cold}, \qquad \textit{Eq. 3}$$

Where ΔT_{cold} was the temperature difference between the inlet and outlet on the cold side, i.e., $T_3 - T_2$. c_f, ρ_f and $\dot{V}$ were the specific heat capacity, the density, and the volume flow rate of the fluid, respectively. The relative standard uncertainty of the cooling power was about 10 %, estimated using the TSM

propagation approach [55]. The stated standard uncertainty was obtained from combining random and systematic uncertainties. While the random uncertainty was determined directly from the experimental data using the standard deviation of the mean, the term accuracy of an instrumentation sensor, as provided by the manufacturer (Table 2), was interpreted and used as the systematic uncertainty in measuring that sensor.

The hydraulic pumping power ($\dot{W}_{pump}$) was the product of volume flow rate and pressure drop through the system, hence assuming a pumping efficiency of 1, and it was calculated as follows:

$$\dot{W}_{pump} = \dot{V}(p_1 - p_2 + p_3 - p_4), \qquad \textit{Eq. 4}$$

Where p_1, p_2, and p_3 are the pressures measured in the three manifolds (see Figure 2). The pressure p_4 is atmospheric pressure and is assumed to be zero. The estimated uncertainty of $\dot{W}_{pump}$ was 3 %.

The magnetic power ($\dot{W}_{mag}$) performed on the MCM inside the regenerator is calculated from the shaft power ($\dot{W}_{shaft}$), which is required to rotate the magnet assembly of the magnetocaloric heat pump. $\dot{W}_{mag}$ includes the losses associated with eddy currents induced in the laminated iron ring. Figure 6 shows $\dot{W}_{shaft}$ as a function of the cycle frequency. When the AMRs are installed, the measured shaft power is about 65 W at a frequency of 1 Hz. The values presented for $\dot{W}_{shaft}$ are measured at a zero temperature span in the regenerators. Thus, there is no magnetic power in the AMRs. The measured power is only losses due to eddy currents induced in the laminated iron ring but also bearing and coupling friction, and other losses. We can therefore write:

$$\dot{W}_{mag} = \dot{W}_{shaft} - \dot{W}_{losses}, \qquad \textit{Eq. 5}$$

Where $\dot{W}_{shaft}$ is given by:

$$\dot{W}_{shaft} = 2\pi f \Gamma, \qquad \textit{Eq. 6}$$

The operating frequency, f, is half of the AMR frequency (or cycle frequency), as the magnetic circuit generates two high field regions. The interaction between the magnetic circuit and the regenerator beds (i.e., the magnetization and demagnetization of the beds) produces an alternating torque, similar as described in [56,57]. Hence, the variation of the torque measurements during the sampling period originates from the nature of the AMR cycle and not from random error sources. The uncertainty of the torque (and power) measurements can then be treated as the system uncertainty [57,58].

As indicated in Figure 6, the shaft losses including the eddy current power loss for the laminated iron ring are a function of the AMR frequency. The iron losses ($\dot{W}_{losses}$) can then be approximated by the following second-order polynomial:

$$\dot{W}_{losses} = \alpha\, f^2 + \beta\, f, \qquad \textit{Eq. 7}$$

$$\alpha = 34.8\ Ws^2,$$

$$\beta = 28.6\ Ws.$$

Where the quadratic term is associated with the eddy current power loss and the linear term represents the losses from friction in the bearings, respectively. In the result and discussion section, we subtract the losses from the shaft power and just report $\dot{W}_{mag}$ as the magnetic (or AMR) power with an uncertainty of 2 %.

The second-law efficiency (η_{II}) is commonly used to compare different refrigeration systems operating at different temperature conditions. A high value of η_{II} indicates that the device operates at minimum losses at a certain operating point, which makes it a useful performance indicator. It is a measure of the actual cooling performance relative to the performance under reversible conditions (i.e., the Carnot cooling cycle) and is given by:

$$\eta_{II} = \frac{COP}{COP_{ideal}}. \qquad \textit{Eq. 8}$$

The relative standard uncertainty of the *COP* and η_{II} is 10 %. The ideal or reversible Carnot *COP* (COP_{ideal}) for a cooling cycle is the maximum performance that the device can theoretically obtain. In terms of hot and cold reservoir temperatures, the ideal *COP* of a device operating with constant temperature sources, as defined by the Carnot cycle, is calculated as:

$$COP_{ideal} = \frac{T_{cold}}{T_{hot} - T_{cold}}, \qquad \textit{Eq. 9}$$

It should be stated that the regenerator temperature span (ΔT_{Reg}), which is based on the fluid temperatures exiting the regenerator at the cold and hot end, will always be greater than the reservoir temperature span [56], and hence lead to higher second-law efficiencies. For the most part, in this study, the temperature span is reported as the reservoir temperature span with a relative uncertainty of 1 %.

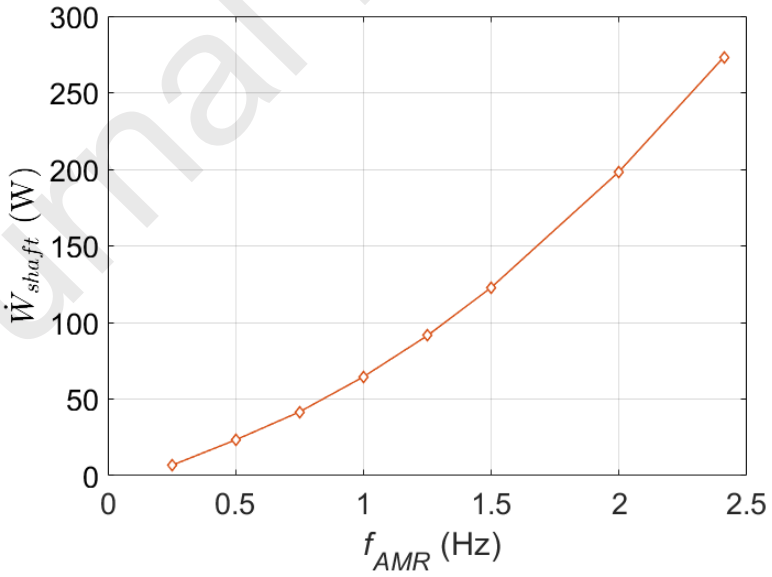

Figure 6: Shaft power as a function of the AMR (cycle) frequency when the AMRs are mounted.

Based on the cooling performance of the AMR device, it is possible to calculate the heating performance of the device, if it is treated as a heat pump. In principle, the heating load supplied to the hot reservoir

(i.e., the heating power, $\dot{Q}_h$) equals the heat removed from the cold reservoir (i.e., the cooling power, $\dot{Q}_c$) plus the input power. Hence, the heat pump *COP* (or heating *COP*) is always 1 greater than the COP of the refrigeration cycle (or cooling *COP*). It should be stated that operating the solenoid valves will cause some heat dissipation to the fluid on the regenerator hot side, which would slightly increase the heating power. However, the heat dissipation is assumed small and hence neglected to avoid overestimating the system performance.

4. Results and discussion

The AMR performance is highly dependent on the MCE of the refrigerant material and the effectiveness of the regenerator bed. The MCE depends on parameters such as the magnitude of the magnetic field, rate of change and orientation of the applied field, and the magnetic and physical properties of the MCM. On the other hand, the effectiveness depends on the AMR bed characteristics, such as porosity, geometry, thermal capacity, and the operating conditions, e.g., utilization factor, frequency, and reservoir temperatures. For an active regenerator, the timing between the field change and fluid flow is critical. Most of the parameters are fixed in the AMR prototype, such as AMR geometry and magnetic field strength. It is hence important to characterize the effects of the remaining variable parameters of the system, such as the individual blow fractions, utilization factor, cycle frequency, and hot and cold reservoir temperatures, to map out the performance. A series of AMR tests was performed at different steady-state operating conditions to characterize those parameters. For analyzing the AMR performance, we also defined the utilization factor (*U*), which is the ratio of the thermal capacity of the working fluid flowing through the regenerator during one blow (cold/hot blow) and the thermal capacity of the solid-state material in the regenerator:

$$U = \frac{\rho_f \, c_{p,f} \, \dot{V}}{2 \, f \, m_s \, c_{p,s}}, \qquad \textit{Eq. 10}$$

Since the amount of ENTEK-FNE in the solution is quite small, only the properties of pure water are used in Eq. 10. The total mass of the MCM is m_s = 3.41 kg. The specific heat capacity of the MCM is set to $c_{p,s}$ = 500 J kg^{-1} K^{-1}, which is the background value (see Figure 4a), as the peak in the FOPT is mostly latent heat [59].

4.1. Varying the average blow fraction

The variation of the blow fraction (or flow waveform), as indicated in Figure 3, is implemented by increasing or reducing the opening period of the solenoid valves, and its effect on the performance of MagQueen was experimentally studied. Two sets of solenoid valves were used in MagQueen to control the cold blow and hot blow fractions (see Figure 2). The effect of varying the average hot blow fractions while keeping the cold blow fraction constant at an average of around 34 % is summarized in Figure 7a and Figure 7b. Tests are run at a constant flow rate of 1300 L/h (*U*=0.40), a cycle frequency of 1.1 Hz, and a hot end temperature of 294 K. At the lowest hot blow fraction, the largest reservoir temperature span of 6.0 K was achieved, while the span at higher blow fractions was around 5.6 K. Furthermore, increasing the hot blow fraction increases the *COP* of the AMR prototype.

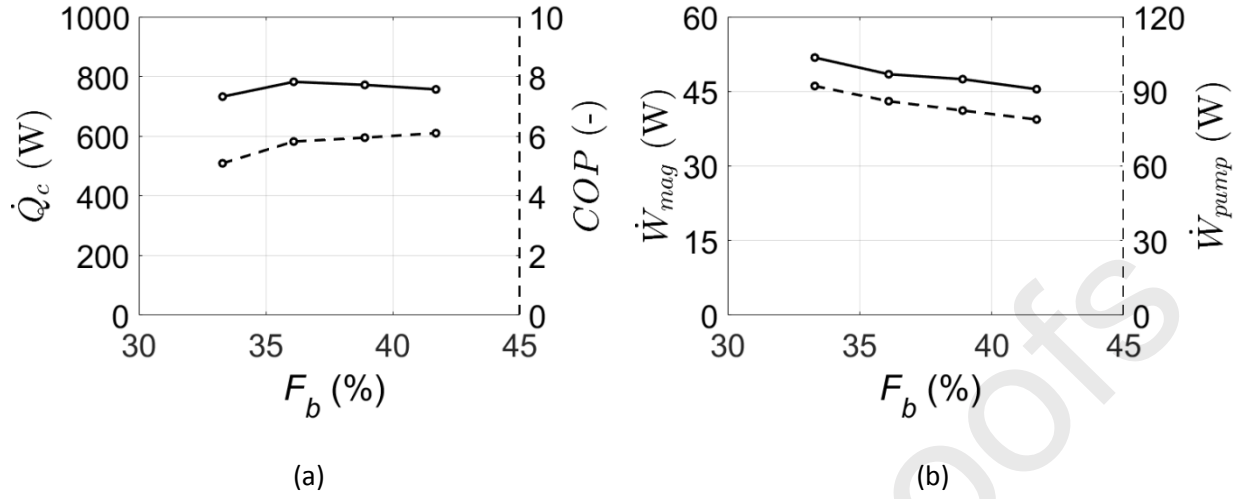

Figure 7: (a) Cooling power (solid line) and cooling COP (dashed line) as a function of the hot blow fraction. (b) Magnetic power (solid line) and pumping power (dashed line) as a function of the hot blow fraction.

To keep the utilization constant irrespectively of the hot blow fraction, the centrifugal pump provides a constant fluid flow rate of 1300 L/h. In the case of a constant flow rate, the pressure drop over each valve will decrease as the hot blow fraction (i.e., the valve opening) increases. In particular, the flow area will increase as the blow fraction increases, while the pressure drop decreases. This results in a reduced system pressure drop and hence a lower pumping power (Figure 7b). It is also important to notice an increase in the magnetic power for a decreasing blow fraction, which was also reported by Nakashima et al. [40]. The authors suggested that the MCM will perform an AMR thermodynamic cycle closer to the ideal Brayton cycle at lower blow fractions, which demands the largest magnetic work.

Figure 7a also shows that it is possible to trade a lower cooling power for a higher *COP*. However, the cooling power and *COP* seem to be balanced well at a hot blow fraction of around 36 %. The results are also in agreement with [11], where it was shown that lower blow fractions give a greater temperature span but lower *COP*s for similar conditions. It should be further stated that the blow fraction is varied based on a fixed utilization, which is similar to the analyses in [11,39–41]. Hence, the optimum blow fraction will change in accordance with the cycle frequency and fluid flow rate. In future studies, the combined effect of cold blow and hot blow fraction variations on the AMR performance should be explored to investigate the impact of flow imbalances during the cold and hot blow, as experienced, for example, by Holladay et al. [42].

4.2. Varying the utilization factor

Practically, the optimum utilization factor depends on many parameters, such as MCM thermal conduction, heat transfer between fluid and refrigerant, temperature span, etc. [23] The dependence of the cooling power and the *COP* on the utilization factor is demonstrated in Figure 8a. The cold and hot reservoir temperatures are 281 K and 295 K, respectively, giving a constant temperature span of 14 K. The fluid flow rate was varied from 400 to 600 L/h (U = 0.27 to 0.40) while keeping the cycle frequency and average blow fractions in both directions constant at 0.5 Hz and 28 %, respectively. For the given span, the cooling power increases with the utilization factor up to an optimum and then decreases quickly. The

highest cooling power of 176.1 W was found at *U* = 0.38, suggesting that this utilization is best to achieve a better trade-off between high cooling power and heat regeneration.

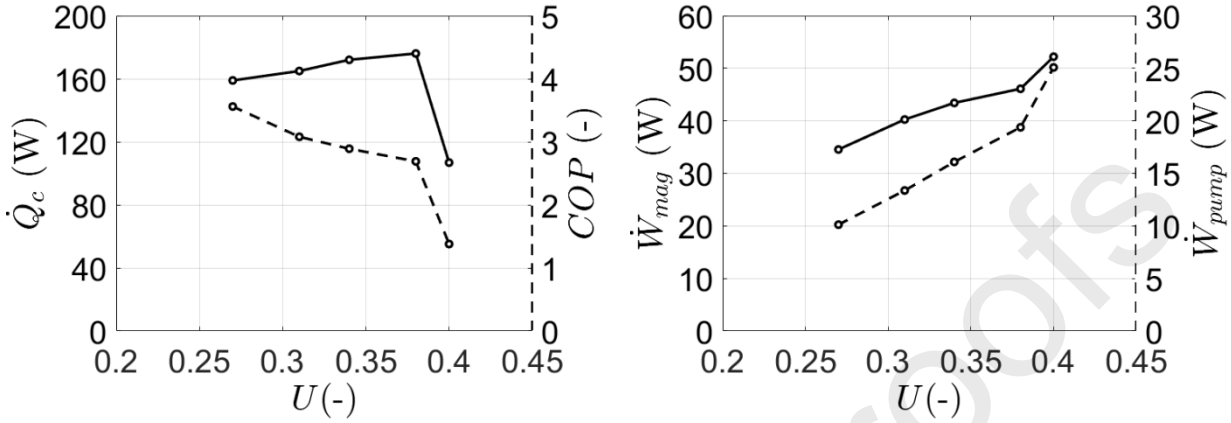

(a) (b)

Figure 8: (a) Cooling power (solid line) and cooling COP (dashed line) as a function of the utilization. (b) Magnetic power (solid line) and pumping power (dashed line) versus the utilization.

If the utilization factor is too small, no useful cooling is generated, as the effect of the heat transfer fluid on the refrigerant temperature is too small. On the other hand, if the utilization exceeds a certain value (i.e., there is too much fluid flow), the thermal gradient drops [60], causing a rapid reduction of the cooling power. It is also shown that the *COP* decreases with increasing utilization factor, which is mainly due to the increasing magnetic power needed for the magnetization/demagnetization of the solid refrigerant (see Figure 8b). As demonstrated by Kitanovski et al. [2], the increase in the magnetic power may be attributed to a higher degree of overlapping of the internal (local) thermodynamic cycles between the adjacent particles of the magnetocaloric material inside the regenerators. Although the pumping power increases as a result of higher volume flow rates (i.e., higher utilization factors), the contribution of the magnetic power to the *COP* is about three times greater than the pumping power. However, it can be expected that higher cycle frequencies (and hence higher flow rates) will result in a greater pumping work.

4.3. Varying the hot reservoir temperature

Keeping the cycle frequency at 0.5 Hz, the blow fractions in both directions at 28 %, and the flow rate at around 500 L/h (*U* = 0.34), the hot and cold reservoir temperatures were varied, while the cooling power and cooling *COP* were measured. These results are summarized in Figure 9a and Figure 9b. Under these conditions, the highest cooling powers are obtained at a hot reservoir temperature of 295 K. In particular, a maximum cooling power of about 288 W at a temperature span of 10.3 K could be achieved. The cooling *COP* is quite sensitive to the hot reservoir temperature applied as well as to the temperature span. Under these test conditions, the highest second-law efficiency of 20.6 % was obtained at a hot reservoir temperature of 295 K. In this case, the temperature span and cooling *COP* were 10.3 K and 5.7, respectively.

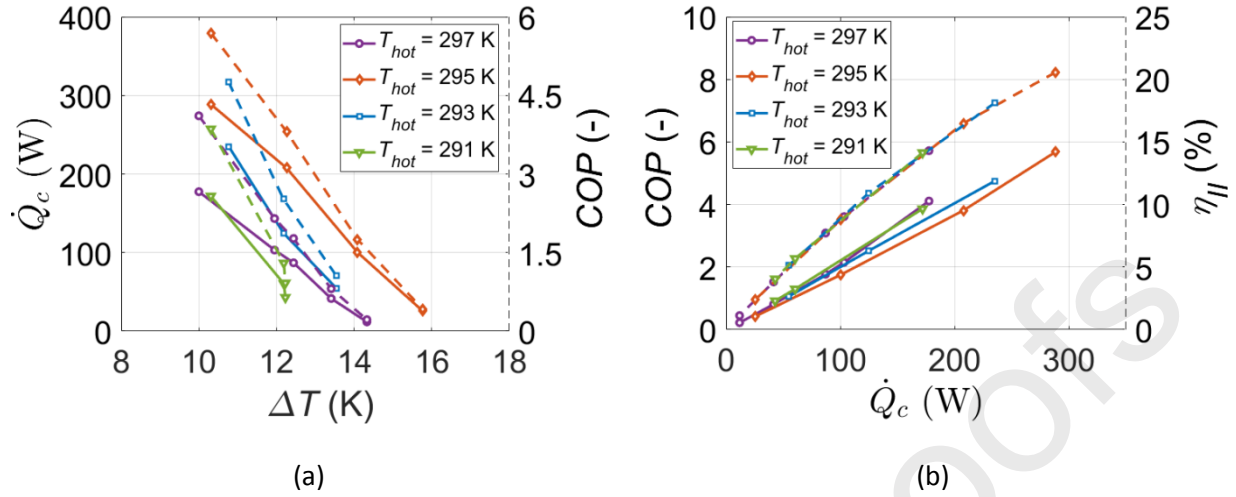

(a) (b)

Figure 9: (a) Cooling power (solid lines) and cooling COP (dashed lines) vs. temperature span at different hot reservoir working temperatures. (b) Cooling performance maps (cooling COP vs. cooling power) for different hot reservoir temperatures at a cycle frequency of 0.5 Hz. The cooling COP is plotted with solid lines, while the second-law efficiency is plotted with dashed lines.

Figure 10a shows the thermal loads as a function of established temperature span for different hot reservoir temperatures. The AMR performance is quite sensitive to the hot reservoir temperature. It can be seen that the AMR device has an optimum hot reservoir temperature at 295 K, where the magnetocaloric effect over the entire regenerator is maximized and hence reaches a maximum temperature span. The maximum temperature span is achieved at a hot reservoir temperature that is slightly higher than the hottest T_{Curie} of 292 K of the multi-layer AMR beds. The occurrence of the maximum temperature span at a hot reservoir temperature above the T_{Curie} was also described in [61], and it can be explained by the temperature shift between the maxima of the curves for the adiabatic temperature change upon magnetization and demagnetization [62]. For thermal loads of 100 W and 200 W, the maximum temperature spans were achieved at the optimum hot reservoir temperature of 295 K.

The cooling performance curves in Figure 9b also show that the AMR device performs much more efficiently at higher cooling power regardless of the hot reservoir temperature. Furthermore, different fluid flow profiles might be desired in different situations. One profile could be optimized for high cooling power, another one for high *COP* during low cooling power operation. At a higher temperature span, the magnetic attraction of the magnetocaloric refrigerant increases, which results in a higher magnetic power. There can be several reasons for this. As the temperature span increases, the material at the cold end of the regenerator starts to operate at temperatures nearer their Curie temperature, where the MCE and change in magnetic energy are largest. There is also a larger thermodynamic work related to transporting heat over a larger temperature span, as indicated by Eq. 9. Finally, as the temperature span increases, the regenerator will become more ferromagnetic, and the increased magnetic force can cause increased friction on the bearings. Furthermore, although not large, the pumping effort at higher spans is greater than at lower spans due to the increased viscosity of the heat transfer fluid at the cold end. As a consequence of the increase in the magnetic power and pumping power, the thermodynamic efficiency of the AMR device at larger temperature spans is reduced. Figure 10b demonstrates this effect. All data

points are produced at a hot reservoir temperature of 295 K, blow fractions in both directions of 28 %, a frequency of 0.5 Hz, and a volume flow rate of 500 L/h (*U*=0.34).

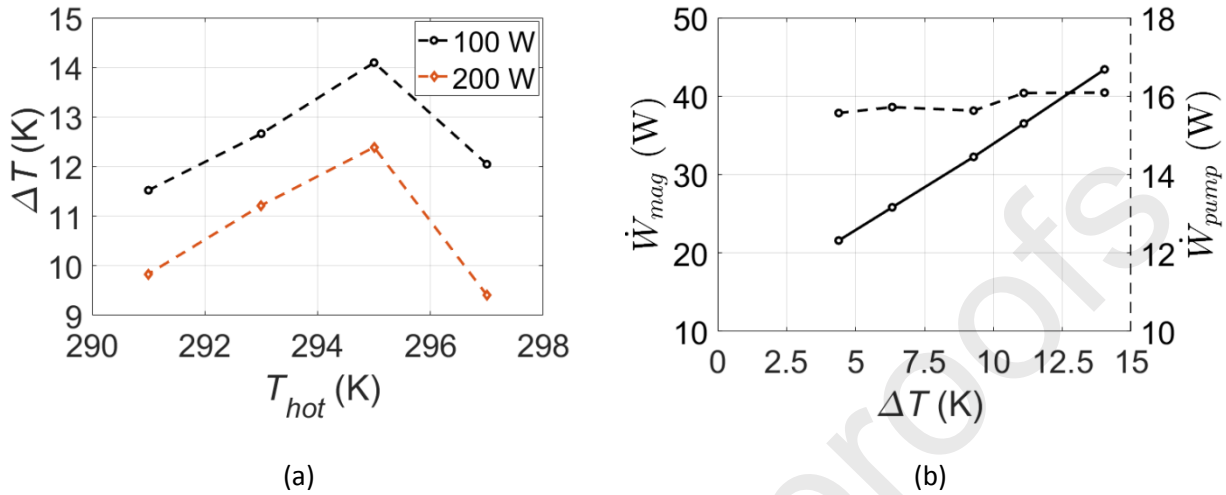

(a) (b)

Figure 10: (a) Temperature span vs. hot reservoir temperature for thermal loads of 100 W and 200 W, from interpolating the data in Figure 9. (b) Magnetic power (solid line) and pumping power (dashed line) versus the temperature span at a fixed hot reservoir temperature of 295 K and a frequency of 0.5 Hz.

4.4. Individual bed optimization

Changing the blow fraction of individual beds makes it possible to correct variations in the respective cold side regenerator outlet temperatures. A similar procedure was demonstrated in [37,38]. Figure 11 shows the cold fluid temperatures exiting the 13 AMRs of MagQueen running at 1.1 Hz, a hot reservoir temperature of 294 K, a flow rate of 800 L/h, and average blow fractions of 36 % in both directions. It should be noted that the experimental data previous to this section was not based on an adjusted flow. It can be seen that after reaching steady-state operation, the fluid exiting regenerator beds #1 and #5 is warmer than the other beds that show a variation of ca. 0.5 K in cold side temperature. It hence appears that the hydraulic resistance through those two beds is different compared to the rest, causing a larger fluid flow during the hot blow period. At this point, the established temperature span across the regenerator (ΔT_{Reg}) was about 8.7 K. After reducing the hot blow fraction for these two beds (i.e., by reducing the valve opening to shorten the hot blow period) and while maintaining the same utilization, it was possible to lower the cold outlet fluid temperature exiting these beds. As a result, the regenerator temperature span was increased to about 9.0 K. At the same time, the cooling power and *COP* increased from 532.0 W to 557.4 W and 6.86 to 6.92, respectively. The fact that adjusting the flows in the different regenerators has a positive effect on the system performance metrics shows the significance of flow balancing in multi-bed AMR devices and motivates a more detailed investigation of this effect in future studies.

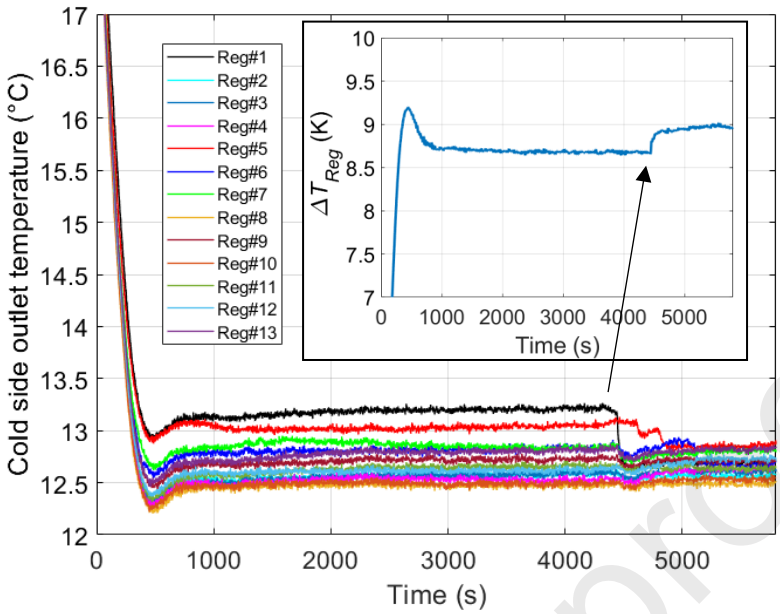

Figure 11: Effect of adjusting the hot blow fraction on the regenerator cold outlet temperature (large figure) and regenerator temperature span (inset). At 4400 s, the hot blow fractions for bed#1 and bed#5 are adjusted.

4.5. Varying the cycle frequency

The performance of MagQueen was also investigated at different cycle frequencies. While maintaining a temperature span of 10.3 K and at a frequency of 0.5 Hz, a flow rate of around 500 L/h (U=0.34), blow fractions of 36 % in both directions, and a T_{hot} = 295 K, the AMR was able to provide a cooling power of about 288 W (Figure 12a). It is worth mentioning that the cooling *COP* and COP_{ideal} for this case were 5.7 and 27.6, respectively. This represents a second-law efficiency of 20.6 % of the heat pump (Figure 12b). In comparison, the rotary AMR system previously developed by DTU obtained a second-law efficiency of 18 % with a cooling *COP* of 3.6 [20]. At a similar temperature span of 9.9 K, but at a frequency of 1.2 Hz, a flow rate of 1060 L/h (U=0.30), blow fractions of 36 % in both directions, and a similar hot reservoir temperature, the AMR produced a cooling power of 477.2 W with a *COP* of 3.8. A maximum cooling power of 814.7 W was obtained while maintaining a 5.7 K-span at 1.2 Hz and a flow rate of 1280 L/h (U=0.36). In this case, the cooling *COP* and η_{II} were 6.04 and 11.6 %, respectively. For this set of experiments, flow adjustments in the different beds, similar to Figure 11, were only made for experiments run at 1.2 Hz. Tests at higher frequencies were not performed at similar greater temperature spans as for 0.5 Hz to reduce the risks of experiencing large torque that could damage the mechanical couplings.

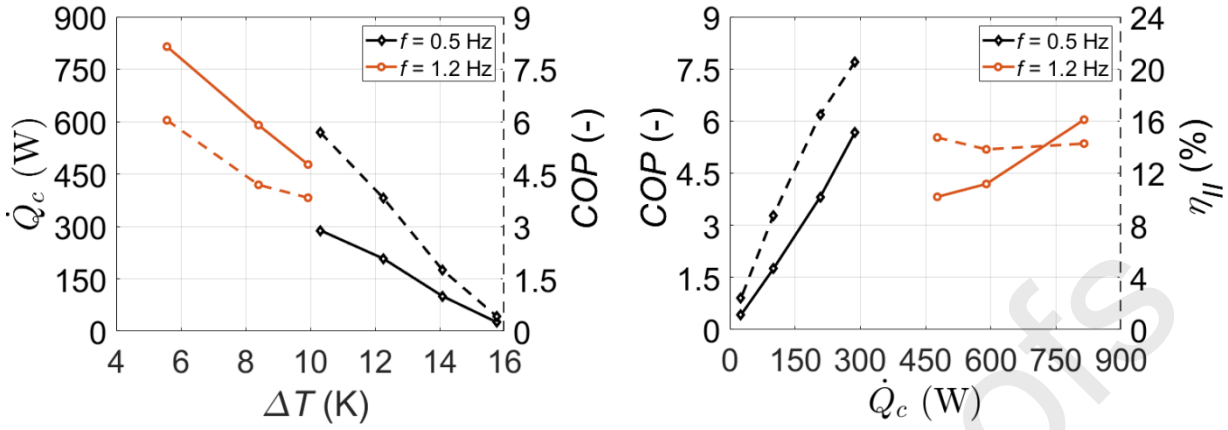

Figure 12: (a) Cooling power (solid lines) and cooling COP (dashed lines) vs. temperature span at different cycle frequencies. (b) Cooling performance maps (cooling COP vs. cooling power) for different cycle frequencies. The cooling COP is plotted with solid lines, while the second-law efficiency is plotted with dashed lines.

Operating MagQueen at higher cycle frequencies is accompanied by a lower *COP* because of an increased pumping work due to a greater flow rate and larger shaft power needed to rotate the magnet assembly. For example, at 1.2 Hz and a span of around 10 K, the pumping power was about 57 W to push the fluid with a flow rate of 1060 L/h (*U*=0.30) through the AMR system, while it was only 13 W for a flow of 500 L/h (*U*=0.34) at 0.5 Hz and a 10.3 K-span. The large reduction of the pumping power resulted from a lower fluid flow rate and decreased system pressure drop. The heat pump operation at higher cycle frequencies was limited due to the increasing pressure drop through the regenerator beds, which ultimately limited the system efficiency. Alternative regenerator geometries with reduced hydraulic resistance, such as thin parallel plates [63,64] or microchannels [65], offer a better heat transfer to pressure drop ratio and may reach higher system efficiencies.

5. Stability of the magnetocaloric material

It is of practical importance for manufacturers to develop stable and efficient magnetocaloric refrigerants that can eventually be commercialized in future caloric applications. Commonly, $La(Fe,Si)_{13}$-based compounds tend to have low mechanical strength due to both the intrinsic brittleness of the 1:13 phase [66] and the magnetovolume effects that cause a volume expansion (ca. 1 % [67]) during the phase transition. Previous studies have shown that mixing the MCM with epoxy resin [59,68–70] or metal binders [71] improved the mechanical strength of such compounds by enhancing the binding force between neighboring particles.

In the present work, the $La(Fe,Si)_{13}$-based compound has no epoxy or metal binder. Instead, the mechanical properties of the CALORIVAC-HS material were improved by increasing the content of the ductile α-Fe phase, which was shown to solve the brittleness issue of the 1:13 phase [72]. To assess the mechanical and chemical stability of the non-bonded refrigerant, the specific heat capacity measurement was repeated after an extended test period of 170 hours (about 490,000 cycles based on an average test frequency of 0.8 Hz). The data are shown in Figure 13. It is observed that the peaks after testing are slightly

higher and at slightly lower temperatures. This is ascribed to uncertainties when selecting small amounts of material for testing. Due to the chemical distribution known to exist, the average Curie temperature of a small amount of sample may vary slightly. Furthermore, a photograph of the bed material after the testing period shows good mechanical integrity, as the particles retained their shape and did not disintegrate or oxidize during testing. It can hence be concluded that the CALORIVAC-HS material offers good long-term stability.

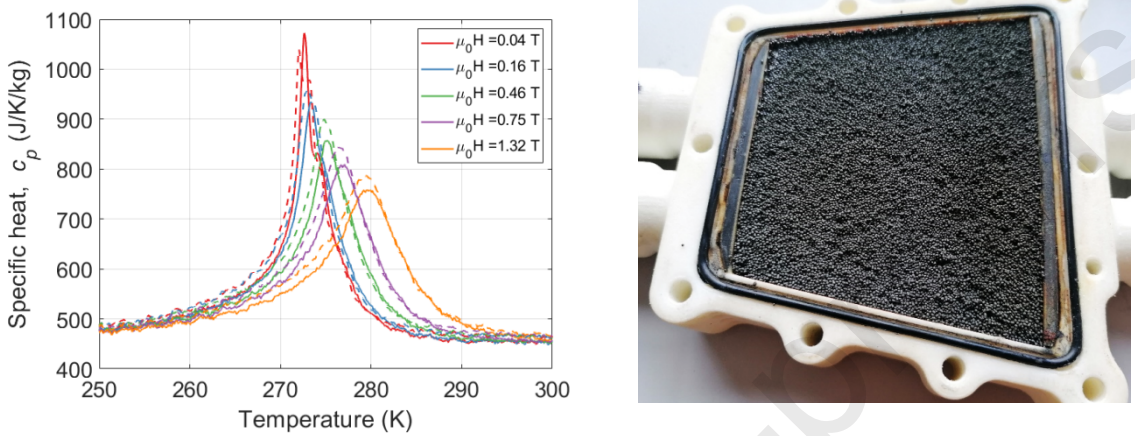

Figure 13: (a) Specific heat capacity curves for one MCM layer before (solid line) and after (dashed line) testing. (b) AMR bed opened after an extended test period of 170 hours. No sign of particle oxidation or disintegration.

6. Conclusions

The MagQueen prototype built by DTU is designed as a functional rotary magnetocaloric heat pump that can operate with high efficiency using ten alloys of $La(Fe,Mn,Si)_{13}H_y$ as the magnetocaloric refrigerant. At a cycle frequency of 1.2 Hz, the device produced a maximum of 815 W cooling power over a reservoir temperature span of 5.6 K with a cooling *COP* of 6.0. A peak second-law efficiency of 20.5 % (*COP* = 5.7) was obtained at a cooling power of about 288 W and a 10.3 K temperature span while operating at a cycle frequency of 0.5 Hz. The experimental results are comparable with other state-of-the-art active magnetic refrigerators. The device can control the flow through each of the 13 regenerator beds, enabling great freedom to control the magnetic refrigeration cycle, such as adjusting the blow periods and AMR cycle time. Increasing the blow fractions for selected regenerators was shown to improve the temperature span for a fixed utilization. Furthermore, it was observed that flow imbalances in different regenerators could reduce system performance metrics. A method to correct flow imbalances was presented, leading to enhanced cooling capacity and efficiency. It encourages a more thorough investigation of the effect of flow balancing in future studies.

Acknowledgements

This work was in part financed by the RES4Build project, which received funding from the European Union's Horizon 2020 research and innovation program under grant agreement No. 814865. We would like to acknowledge the ENOVHEAT project funded by the Innovation Fund Denmark (contract no 12-132673). We also wish to acknowledge Mike Wichmann for the technical support and Vacuumschmelze GmbH & Co. KG (Germany) for providing the magnetocaloric materials for this work.

References

[1] C. Arpagaus, F. Bless, M. Uhlmann, J. Schiffmann, S.S. Bertsch, High temperature heat pumps: Market overview, state of the art, research status, refrigerants, and application potentials, Energy. 152 (2018) 985–1010. doi:10.1016/j.energy.2018.03.166.

[2] A. Kitanovski, J. Tušek, U. Tomc, U. Plaznik, M. Ožbolt, A. Poredoš, Magnetocaloric Energy Conversion : From Theory to Applications, Springer, 2015.

[3] M. Waite, E. Cohen, H. Torbey, M. Piccirilli, Y. Tian, V. Modi, Global trends in urban electricity demands for cooling and heating, Energy. 127 (2017) 786–802. doi:10.1016/j.energy.2017.03.095.

[4] W. Goetzler, R. Shandross, J. Young, O. Petritchenko, D. Ringo, S. McClive, Energy Savings Potential and RD&D Opportunities for Commercial Building HVAC Systems, 2017. doi:10.2172/1419622.

[5] D.R. Brown, T.B. Stout, J.A. Dirks, N. Fernandez, The prospects of alternatives to vapor compression technology for space cooling and food refrigeration applications, Energy Eng. J. Assoc. Energy Eng. 109 (2012) 7–20. doi:10.1080/01998595.2012.10554226.

[6] K.L. Engelbrecht, G.F. Nellis, S.A. Klein, A Numerical Model of an Active Magnetic Regenerator Refrigeration System, in: Cryocoolers 13, Springer US, Boston, USA, 2005: pp. 471–480. doi:10.1007/0-387-27533-9_60.

[7] P. V. Trevizoli, T. V. Christiaanse, P. Govindappa, I. Niknia, R. Teyber, J.R. Barbosa Jr., A. Rowe, Magnetic heat pumps: An overview of design principles and challenges, Sci. Technol. Built Environ. 22 (2016) 507–519. doi:10.1080/23744731.2016.1171632.

[8] J.A. Barclay, Use of a ferrofluid as the heat-exchange fluid in a magnetic refrigerator, J. Appl. Phys. 53 (1982) 2887–2894. doi:10.1063/1.331069.

[9] K.K. Nielsen, C.R.H. Bahl, A. Smith, R. Bjørk, N. Pryds, J. Hattel, Detailed numerical modeling of a linear parallel-plate Active Magnetic Regenerator, Int. J. Refrig. 32 (2009) 1478–1486. doi:10.1016/j.ijrefrig.2009.03.003.

[10] D. Eriksen, Active magnetic regenerator refrigeration with rotary multi-bed technology, (2016) 161.

[11] F.P. Fortkamp, D. Eriksen, K. Engelbrecht, C.R.H. Bahl, J.A. Lozano, J.R. Barbosa Jr., Experimental investigation of different fluid flow profiles in a rotary multi-bed active magnetic regenerator device, Int. J. Refrig. 91 (2018) 46–54. doi:10.1016/j.ijrefrig.2018.04.019.

[12] A.T.D. Nakashima, S.L. Dutra, J.R. Barbosa Jr., Experimental Evaluation of the Flow Imbalance in an Active Magnetic Experimental, 9th World Conf. Exp. Heat Transf. Fluid Mech. Thermodyn. (2017).

[13] A. Tura, A. Rowe, Permanent magnet magnetic refrigerator design and experimental characterization, Int. J. Refrig. 34 (2010) 628–639. doi:10.1016/j.ijrefrig.2010.12.009.

[14] K. Engelbrecht, D. Eriksen, C.R.H. Bahl, R. Bjørk, J. Geyti, J.A. Lozano, K.K. Nielsen, F. Saxild, A. Smith, N. Pryds, Experimental results for a novel rotary active magnetic regenerator, Int. J. Refrig. 5 (2012) 3–10. doi:10.1016/j.ijrefrig.2012.05.003.

[15] J. Tušek, S. Zupan, A. Šarlah, I. Prebil, A. Poredos, Development of a rotary magnetic refrigerator, Int. J. Refrig. 33 (2010) 294–300. doi:10.1016/j.ijrefrig.2009.11.003.

[16] D. Eriksen, K. Engelbrecht, C.R.H. Bahl, R. Bjørk, K.K. Nielsen, A.R. Insinga, N. Pryds, Design and experimental tests of a rotary active magnetic regenerator prototype, Int. J. Refrig. 58 (2015) 14–

21. doi:10.1016/j.ijrefrig.2015.05.004.

[17] C. Aprea, A. Greco, A. Maiorino, C. Masselli, The energy performances of a rotary permanent magnet magnetic refrigerator, Int. J. Refrig. 61 (2016) 1–11. doi:10.1016/j.ijrefrig.2015.09.005.

[18] J.A. Lozano, K. Engelbrecht, C.R.H. Bahl, K.K. Nielsen, D. Eriksen, U.L. Olsen, J.R. Barbosa Jr., A. Smith, A.T. Prata, N. Pryds, Performance analysis of a rotary active magnetic refrigerator, Appl. Energy. 111 (2013) 669–680. doi:10.1016/j.apenergy.2013.05.039.

[19] J. Tušek, A. Kitanovski, S. Zupan, I. Prebil, A. Poredoš, A comprehensive experimental analysis of gadolinium active magnetic regenerators, Appl. Therm. Eng. 53 (2013) 57–66. doi:10.1016/j.applthermaleng.2013.01.015.

[20] D. Eriksen, K. Engelbrecht, C.R.H. Bahl, R. Bjørk, Exploring the efficiency potential for an active magnetic regenerator Exploring the efficiency potential for an active magnetic regenerator, Sci. Technol. Built Environ. 22 (2016) 527–533. doi:10.1080/23744731.2016.1173495.

[21] C.R.H. Bahl, K. Engelbrecht, D. Eriksen, J.A. Lozano, R. Bjørk, J. Geyti, K.K. Nielsen, A. Smith, N. Pryds, Development and experimental results from a 1 kW prototype AMR, Int. J. Refrig. 37 (2013) 78–83. doi:10.1016/j.ijrefrig.2013.09.001.

[22] S. Lionte, M. Risser, C. Muller, A 15 kW magnetocaloric proof-of-concept unit: initial development and first experimental results, Int. J. Refrig. (2020). doi:10.1016/j.ijrefrig.2020.09.019.

[23] Z. Li, J. Shen, K. Li, X. Gao, X. Guo, W. Dai, Assessment of three different gadolinium-based regenerators in a rotary-type magnetic refrigerator, Appl. Therm. Eng. 153 (2019) 159–167. doi:10.1016/j.applthermaleng.2019.02.100.

[24] S.Y. Dan'Kov, A.M. Tishin, V.K. Pecharsky, K.A. Gschneidner Jr., Magnetic phase transitions and the magnetothermal properties of gadolinium, Phys. Rev. B. 57 (1998) 3478–3490. doi:10.1103/PhysRevB.57.3478.

[25] A. Smith, C.R.H. Bahl, R. Bjork, K. Engelbrecht, K.K. Nielsen, N. Pryds, Materials challenges for high performance magnetocaloric refrigeration devices, Adv. Energy Mater. 2 (2012) 1288–1318. doi:10.1002/aenm.201200167.

[26] T. Lei, K. Engelbrecht, K.K. Nielsen, H. Neves, Optimization of Multi-layer Active Magnetic Regenerator towards Compact and Efficient Refrigeration, 29th Int. Conf. Effic. Cost, Optimisation, Simul. Environ. Impact Energy Syst. (2016) 1–12.

[27] T. Lei, K. Engelbrecht, K.K. Nielsen, H. Neves Bez, C.R.H. Bahl, Study of multi-layer active magnetic regenerators using magnetocaloric materials with first and second order phase transition, J. Phys. D. Appl. Phys. 49 (2016). doi:10.1088/0022-3727/49/34/345001.

[28] S. Jacobs, J. Auringer, A. Boeder, J. Chell, L. Komorowski, J. Leonard, S. Russek, C. Zimm, The performance of a large-scale rotary magnetic refrigerator, Int. J. Refrig. 37 (2013) 84–91. doi:10.1016/j.ijrefrig.2013.09.025.

[29] S. Lionte, A. Barcza, M. Hittinger, M. Risser, C. Muller, M. Katter, Recent experimental results of first order LaFeSi-based magnetocaloric materials in an Active Magnetic Regeneration device, in: Refrig. Sci. Technol., 2018: pp. 56–61. doi:10.18462/iir.thermag.2018.0008.

[30] B. Monfared, B. Palm, New magnetic refrigeration prototype with application in household and professional refrigerators, in: Refrig. Sci. Technol., 2016: pp. 146–149. doi:10.18462/iir.thermag.2016.0142.

[31] S. Dall'Olio, D. Eriksen, K. Engelbrecht, A.R. Insinga, C.R.H. Bahl, Design, enhanced thermal and flow efficiency of a 2 kW active magnetic regenerator, in: 9th World Conf. Exp. Heat Transf. Fluid Mech. Thermodyn., 2017: pp. 1–10.

[32] G. Sota, T. Kawanami, K. Yamashita, T. Onishi, K. Soejima, H. Wada, S. Hirano, T. Okamura, S. Bae, N. Hirano, K. Shirai, S. Hirasawa, Performance analysis of magnetocaloric heat pump with manganese-based compounds as a magnetic refrigerant, in: Ecos 2016 - Proc. 29th Int. Conf. Effic. Cost, Optimisation, Simul. Environ. Impact Energy Syst., 2016.

[33] L.M. Maier, P. Corhan, A. Barcza, H.A. Vieyra, C. Vogel, J.D. Koenig, O. Schäfer-Welsen, J. Wöllenstein, K. Bartholomé, Active magnetocaloric heat pipes provide enhanced specific power of caloric refrigeration, Commun. Phys. 3 (2020) 186. doi:10.1038/s42005-020-00450-x.

[34] B. Yu, M. Liu, P.W. Egolf, A. Kitanovski, A review of magnetic refrigerator and heat pump prototypes built before the year 2010, Int. J. Refrig. 33 (2010) 1029–1060. doi:10.1016/j.ijrefrig.2010.04.002.

[35] K.A. Gschneidner Jr., V.K. Pecharsky, Thirty years of near room temperature magnetic cooling: Where we are today and future prospects, Int. J. Refrig. 31 (2008) 945–961. doi:10.1016/j.ijrefrig.2008.01.004.

[36] A. Greco, C. Aprea, A. Maiorino, C. Masselli, A review of the state of the art of solid-state caloric cooling processes at room-temperature before 2019, Int. J. Refrig. 106 (2019) 66–88. doi:10.1016/j.ijrefrig.2019.06.034.

[37] D. Eriksen, K. Engelbrecht, C.R.H. Bahl, R. Bjørk, K.K. Nielsen, Effects of flow balancing on active magnetic regenerator performance, Appl. Therm. Eng. 103 (2016) 1–8. doi:10.1016/j.applthermaleng.2016.03.001.

[38] D. Eriksen, K. Engelbrecht, C. Bahl, R. Bjørk, K. Nielsen, A. Insinga, S. Dallolio, N. Pryds, Experimental studies with an active magnetic regenerating refrigerator, Refrig. Sci. Technol. (2015) 926–933. doi:10.18462/iir.icr.2015.0812.

[39] R. Teyber, P.V. Trevizoli, I. Niknia, T.V. Christiaanse, P. Govindappa, A. Rowe, Experimental performance investigation of an active magnetic regenerator subject to different fluid flow waveforms, Int. J. Refrig. 74 (2017) 38–46. doi:10.1016/j.ijrefrig.2016.10.001.

[40] A.T.D. Nakashima, S.L. Dutra, P. V. Trevizoli, J.R. Barbosa Jr., Influence of the flow rate waveform and mass imbalance on the performance of active magnetic regenerators. Part II: Numerical simulation, Int. J. Refrig. 93 (2018) 159–168. doi:10.1016/j.ijrefrig.2018.07.005.

[41] A.T.D. Nakashima, S.L. Dutra, P. V. Trevizoli, J.R. Barbosa Jr., Influence of the flow rate waveform and mass imbalance on the performance of active magnetic regenerators. Part I: Experimental analysis, Int. J. Refrig. 93 (2018) 236–248. doi:10.1016/j.ijrefrig.2018.07.004.

[42] J. Holladay, R. Teyber, K. Meinhardt, E. Polikarpov, E. Thomsen, C. Archipley, J. Cui, J. Barclay, Investigation of bypass fluid flow in an active magnetic regenerative liquefier, Cryogenics (Guildf). 93 (2018) 34–40. doi:10.1016/j.cryogenics.2018.05.010.

[43] H. Johra, K. Filonenko, P. Heiselberg, C. Veje, S. Dall'Olio, K. Engelbrecht, C. Bahl, Integration of a magnetocaloric heat pump in an energy flexible residential building, Renew. Energy. 136 (2019) 115–126. doi:10.1016/j.renene.2018.12.102.

[44] H. Johra, K. Filonenko, P. Heiselberg, C. Veje, T. Lei, S. Dall'Olio, K. Engelbrecht, C. Bahl, Integration of a magnetocaloric heat pump in a low-energy residential building, Build. Simul. 11 (2019) 115–126. doi:10.1007/s12273-018-0428-x.

[45] S. Dall'Olio, M. Masche, J. Liang, A.R. Insinga, D. Eriksen, R. Bjørk, H. Vieyra, A. Barcza, K. Engelbrecht, K.K. Nielsen, H.N. Bez, C. Bahl, Novel design of a high efficiency multi-bed active magnetic regenerator heat pump, Manuscript under review, 2021.

[46] L. Griffith, A. Czernuszewicz, J. Slaughter, V. Pecharsky, Active magnetic regenerative cooling with smaller magnets, Int. J. Refrig. 125 (2021) 44–51. doi:10.1016/j.ijrefrig.2021.01.018.

[47] Z. Li, K. Li, X. Guo, X. Gao, W. Dai, M. Gong, J. Shen, Influence of timing between magnetic field and fluid flow in a rotary magnetic refrigerator, Appl. Therm. Eng. 187 (2021). doi:10.1016/j.applthermaleng.2020.116477.

[48] J. Liang, M. Masche, K. Engelbrecht, K.K. Nielsen, H.A. Vieyra, A. Barcza, C.R.H. Bahl, Experimental study of non-bonded packed bed active magnetic regenerators with stabilized La(Fe,Mn,Si)13Hy particles, Appl. Therm. Eng. 197 (2021) 117383. doi:10.1016/j.applthermaleng.2021.117383.

[49] K.K. Nielsen, H.N. Bez, L. von Moos, R. Bjørk, D. Eriksen, C.R.H. Bahl, Direct measurements of the magnetic entropy change, Rev. Sci. Instrum. 86 (2015) 103903. doi:10.1063/1.4932308.

[50] J.Y. Law, V. Franco, L.M. Moreno-Ramírez, A. Conde, D.Y. Karpenkov, I. Radulov, K.P. Skokov, O. Gutfleisch, A quantitative criterion for determining the order of magnetic phase transitions using the magnetocaloric effect, Nat. Commun. 9 (2018) 2680. doi:10.1038/s41467-018-05111-w.

[51] Vacuumschmelze Gmbh & Co. KG, Magnetocaloric Materials - CALORIVAC, (2015). https://vacuumschmelze.de/Assets-Web/CALORIVAC-PCV-001_2015.pdf (accessed March 3, 2021).

[52] S. Ergun, Fluid Flow through Packed Column, Chem. Eng. Prog. 48 (1952) 125–127.

[53] R.M. Fand, B.Y.K. Kim, A.C.C. Lam, R.T. Phan, Resistance to the flow of fluids through simple and complex porous media whose matrices are composed of randomly packed spheres, J. Fluids Eng. Trans. ASME. 109 (1987) 268–273. doi:10.1115/1.3242658.

[54] D. Nemec, J. Levec, Flow through packed bed reactors: 1. Single-phase flow, Chem. Eng. Sci. 60 (2005) 6947–6957. doi:10.1016/j.ces.2005.05.068.

[55] H.W. Coleman, W.G. Steele, Uncertainty Analysis for Engineers Uncertainty Analysis for Engineers, 2018.

[56] P. V Trevizoli, A.T. Nakashima, G.F. Peixer, J.R. Barbosa Jr., Performance evaluation of an active magnetic regenerator for cooling applications – part I : Experimental analysis and thermodynamic performance, Int. J. Refrig. 72 (2016) 192–205. doi:10.1016/j.ijrefrig.2016.07.009.

[57] J.A. Lozano, Designing a rotary magnetic refrigerator (PhD thesis), (2015).

[58] P.M. de Oliveira, On Air-Water Two-Phase Flows in Return Bends, (2013) 155.

[59] B.P. Vieira, H.N. Bez, M. Kuepferling, M.A. Rosa, D. Schafer, C.C. Plá Cid, H.A. Vieyra, V. Basso, J.A. Lozano, J.R. Barbosa Jr., Magnetocaloric properties of spheroidal La(Fe,Mn,Si)13Hy granules and their performance in epoxy-bonded active magnetic regenerators, Appl. Therm. Eng. 183 (2021) 116185. doi:10.1016/j.applthermaleng.2020.116185.

[60] U. Legait, F. Guillou, A. Kedous-Lebouc, V. Hardy, M. Almanza, An experimental comparison of four magnetocaloric regenerators using three different materials, Int. J. Refrig. 37 (2014) 147–155. doi:10.1016/j.ijrefrig.2013.07.006.

[61] P. V. Trevizoli, J.R. Barbosa Jr., R.T.S. Ferreira, Experimental evaluation of a Gd-based linear

reciprocating active magnetic regenerator test apparatus, Int. J. Refrig. 34 (2011) 1518–1526. doi:10.1016/j.ijrefrig.2011.05.005.

[62] K.K. Nielsen, C.R.H. Bahl, A. Smith, Constraints on the adiabatic temperature change in magnetocaloric materials, Phys. Rev. B - Condens. Matter Mater. Phys. 81 (2010) 1–5. doi:10.1103/PhysRevB.81.054423.

[63] C.R.H. Bahl, K. Navickaitė, H. Neves Bez, T. Lei, K. Engelbrecht, R. Bjørk, K. Li, Z. Li, J. Shen, W. Dai, J. Jia, Y. Wu, Y. Long, F. Hu, B. Shen, Operational test of bonded magnetocaloric plates, Int. J. Refrig. 76 (2017) 245–251. doi:10.1016/j.ijrefrig.2017.02.016.

[64] J. Tušek, A. Kitanovski, A. Poredoš, Geometrical optimization of packed-bed and parallel-plate active magnetic regenerators, Int. J. Refrig. 36 (2013) 1456–1464. doi:10.1016/j.ijrefrig.2013.04.001.

[65] J. Liang, K. Engelbrecht, K.K. Nielsen, K. Loewe, H. Vieyra, A. Barcza, C.R.H. Bahl, Performance assessment of a triangular microchannel active magnetic regenerator, Appl. Therm. Eng. 186 (2021) 116519. doi:10.1016/j.applthermaleng.2020.116519.

[66] J. Lyubina, R. Schäfer, N. Martin, L. Schultz, O. Gutfleisch, Novel Design of La(Fe,Si)13 Alloys Towards High Magnetic Refrigeration Performance, Adv. Mater. 22 (2010) 3735–3739. doi:10.1002/adma.201000177.

[67] A. Fujita, S. Fujieda, K. Fukamichi, H. Mitamura, T. Goto, Itinerant-electron metamagnetic transition and large magnetovolume effects in La(FexSi1-x)13 compounds, Phys. Rev. B - Condens. Matter Mater. Phys. 65 (2002) 144101–144106. doi:10.1103/PhysRevB.65.014410.

[68] H. Zhang, Y. Sun, E. Niu, F. Hu, J. Sun, B. Shen, Enhanced mechanical properties and large magnetocaloric effects in bonded La(Fe, Si) 13 -based magnetic refrigeration materials, Appl. Phys. Lett. 104 (2014) 062407. doi:10.1063/1.4865236.

[69] H. Zhang, Y. Sun, Y. Li, Y. Wu, Y. Long, J. Shen, F. Hu, J. Sun, B. Shen, Mechanical properties and magnetocaloric effects in La(Fe, Si) 13 hydrides bonded with different epoxy resins, J. Appl. Phys. 117 (2015) 063902. doi:10.1063/1.4908018.

[70] T. Lei, K. Navickaitė, K. Engelbrecht, A. Barcza, H. Vieyra, K.K. Nielsen, C.R.H. Bahl, Passive characterization and active testing of epoxy bonded regenerators for room temperature magnetic refrigeration, Appl. Therm. Eng. 128 (2018) 10–19. doi:10.1016/j.applthermaleng.2017.08.152.

[71] I.A. Radulov, D.Y. Karpenkov, K.P. Skokov, A.Y. Karpenkov, T. Braun, V. Brabänder, T. Gottschall, M. Pabst, B. Stoll, O. Gutfleisch, Production and properties of metal-bonded La(Fe,Mn,Si)13Hx composite material, Acta Mater. 127 (2017) 389–399. doi:10.1016/j.actamat.2017.01.054.

[72] J. Wang, Y. Gong, J. Liu, X. Miao, G. Xu, F. Chen, Q. Zhang, F. Xu, Balancing negative and positive thermal expansion effect in dual-phase La(Fe,Si)13/α-Fe in-situ composite with improved compressive strength, J. Alloys Compd. 769 (2018) 233–238. doi:10.1016/j.jallcom.2018.07.349.

Highlights

- **A magnetocaloric device with a parallel flow system was tested by DTU.**
- **The device produced a maximum cooling power of 815 W over a 5.6 K-span at 1.2 Hz.**
- **A maximum second-law efficiency of 20.5 % was achieved.**
- **The device offers great freedom to adjust the cold and hot blow fractions.**

Declaration of interests

☒ The authors declare that they have no known competing financial interests or personal relationships that could have appeared to influence the work reported in this paper.

☐The authors declare the following financial interests/personal relationships which may be considered as potential competing interests: